Journal of Statistical Physics, Vol. 88, Nos. 3/4, 1997

Lyapunov Instability of the Boundary-Driven Chernov–Lebowitz Model for Stationary Shear Flow

Ch. Dellago[1] and H. A. Posch[1]

Received August 5, 1996; final February 27, 1997

We report on the computation of full Lyapunov spectra of the boundary-driven Chernov–Lebowitz model for stationary planar shear flow. The Lyapunov exponents are calculated with a recently developed formalism for systems with elastic hard collisions. Although the Chernov–Lebowitz model is strictly energy conserving, any phase-space volume is subjected to a contraction due to the reflection rules of the hard disks colliding with the walls. Consequently, the sum of Lyapunov exponents is negative. As expected for an inhomogeneously driven system, the Lyapunov spectra do not obey the conjugate pairing rule. The external driving makes the system less chaotic, which is reflected in a decrease of the Kolmogorov–Sinai entropy if the driving is increased.

KEY WORDS: Nonequilibrium steady states; Lyapunov instability; shear flow; computer simulations; many-body hard-disk systems.

1. INTRODUCTION

The response of a fluid system to shear is described by its shear viscosity η. Consider boundary driven planar Couette-flow for which the top and bottom boundaries move in the positive and negative x-directions, respectively. For small boundary velocities a linear velocity profile builds up, and momentum is transported across the flow. The shear viscosity linearly relates the rate of transfer of x-momentum perpendicular to the flow, the xy-component of the stress tensor, to the velocity gradient. To compute η from the microscopic characteristics of a fluid both equilibrium and nonequilibrium molecular dynamics simulations have been extensively used.[1, 2] In the nonequilibrium case two fundamentally different methods

[1] Institut für Experimentalphysik, Universität Wien, A-1090 Vienna, Austria.

0022-4715/97/0800-0825$12.50/0 © 1997 Plenum Publishing Corporation

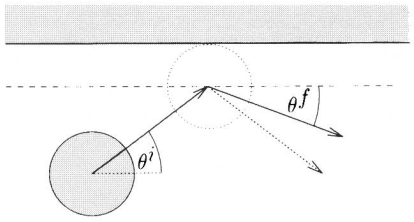

Fig. 1. Geometry of the Chernov–Lebowitz model for a top-wall collision. The square simulation cell with side L is bounded by hard walls on the top and the bottom. Periodic boundary conditions apply in x-direction.

have been applied. The shear flow is induced either directly by moving boundaries acting on Newtonian particles[3] or by "fictitious" mechanical forces coupled homogeneously to the equations of motion of all particles.[4, 5] In both approaches the shearing motion generates heat, which must be removed from the system to avoid heating and to generate a steady state. Provided that a deterministic thermostatting scheme is used, the phase-space distribution collapses onto a multifractal strange attractor, whose information dimension can be considerably less then the original phase-space dimension.[3, 6]

Recently, Chernov and Lebowitz proposed a two-dimensional Hamiltonian model for stationary shear flow.[7] It consists of N identical hard disks of mass m and diameter σ interacting through impulsive hard collisions. The system is periodic in x-direction and bounded by hard reflecting walls in y-direction. Appropriate energy conserving reflection rules at the top and the bottom wall generate a shear flow with an approximately linear velocity profile. As shown in Fig. 1 the momentum of a particle impinging on the top wall is rotated in the direction of the positive x-axis. Analogously, the particle's momentum is rotated towards the negative x-axis at a collision with the bottom wall. These reflection rules increase the x-component of the momentum at the expense of its y-component. Since at the wall collisions the momenta are only rotated while conserving their norm, the model is strictly energy conserving and no thermostat is required. Nevertheless, the model is dissipative in the sense that the phase-space volume occupied by a given distribution is continuously shrinking.

We specify the wall collisions by

$$\begin{aligned} \theta^f &= f_t(\theta^i) \qquad \text{top wall} \\ \theta^f &= f_b(\theta^i) \qquad \text{bottom wall} \end{aligned} \tag{1.1}$$

where θ^i and θ^f are the angles between the momentum direction and the positive x-axis immediately before and after the collision, respectively. If the same reflection rule is used for the top and the bottom wall, a single function $g(\theta)$ defines the reflection for both boundaries:

$$\begin{aligned} \theta^f &= g(\theta^i) && \text{top wall} \\ \theta^f &= \pi + g(\pi + \theta^i) && \text{bottom wall} \end{aligned} \tag{1.2}$$

Chernov and Lebowitz used two particularly simple reflection rules,

$$g(\theta) = -c\theta \tag{1.3}$$

and

$$g(\theta) = -(\pi + b)[(\pi + b)^2 - \theta(\theta + 2b)]^{1/2} \tag{1.4}$$

with $c, b \geqslant 0$ and $c \leqslant 1$. The parameter values $c = 1$ and $b^{-1} = 0$ represent stationary walls with specular reflection, $\theta^f = \theta^i$. Both rules (1.3) and (1.4), which are henceforth referred to as c-rule and b-rule, respectively, induce approximately linear velocity profiles. As noted by Chernov and Lebowitz, the b-rule makes the system retrace its trajectory in configuration space backward after a reversal of the momenta of all particles, a consequence of the time-reversal symmetry of the map (1.4). Note that our definition of the angles differs slightly from that in the original paper.[7]

Due to the dispersing action of the hard collisions the Chernov–Lebowitz model is chaotic in the sense that two infinitesimally separated trajectories diverge exponentially with time. The average logarithmic divergence rates in phase space are described by the so-called Lyapunov exponents λ_l. To give a more rigorous definition of these exponents we consider the phase-space vector $\mathbf{\Gamma} = \{\mathbf{q}_1, \mathbf{q}_2, \mathbf{q}_3, \ldots, \mathbf{q}_N, \mathbf{p}_1, \mathbf{p}_2, \mathbf{p}_3, \ldots, \mathbf{p}_N\}$ containing the $2N$ coordinates and the $2N$ momentum components of all disks. The time evolution

$$\mathbf{\Gamma}(t) = \Phi^t[\mathbf{\Gamma}(0)] \tag{1.5}$$

of an initial state $\mathbf{\Gamma}(0)$ consists of a smooth streaming which is interrupted by collisions between the particles and by collisions of the particles with the walls. Next we consider a satellite trajectory $\mathbf{\Gamma}_s(t)$ initially displaced from the reference trajectory by an infinitesimal vector $\delta\mathbf{\Gamma}(0)$. In a chaotic system $|\delta\mathbf{\Gamma}(t)|$ is growing—on the average—exponentially, causing the system to be unpredictable for long times. According to Oseledec[8] there

exists a complete set of linear-independent initial vectors $\{\delta\mathbf{\Gamma}_l(0); l=1,...,4N\}$ such that the Lyapunov exponents

$$\lambda_l = \lim_{t\to\infty} \frac{1}{t} \ln \frac{|\delta\mathbf{\Gamma}_l(t)|}{|\delta\mathbf{\Gamma}_l(0)|} \tag{1.6}$$

exist. The λ_l, which we order according to $\lambda_1 \geqslant \lambda_2 \geqslant \cdots \geqslant \lambda_{4N}$, are independent of the coordinate system and the metric. The whole set of Lyapunov exponents is referred to as Lyapunov spectrum.

In Hamiltonian systems the Lyapunov exponents appear in pairs summing up to zero, $\lambda_i + \lambda_{4N-i+1} = 0$ for $i=1,...,2N$, due to the symplectic nature of the equations of motion. In a continuous dynamical system the Lyapunov exponent associated with the direction of the phase flow vanishes. Moreover, each conserved quantity causes an additional Lyapunov exponent to vanish. The symmetry found in symplectic dynamical systems is lost if the system is driven to a nonequilibrium stationary state. However, if the system is homogeneously driven, the symmetry is replaced by the so-called *conjugate pairing rule*.[9] According to this rule, the pair sums of the largest and smallest exponents, $\lambda_1 + \lambda_{4N}$, of the next smaller respective larger exponents, $\lambda_2 + \lambda_{4N-1}$, and so forth, are all equal to the same negative value C, provided that the two vanishing exponents associated with the conservation of energy and the nonexponential behavior in flow direction are previously excluded from the ordered list of exponents.[10] There are altogether $2N-1$ of such pairs in our case. For inhomogeneously boundary-driven systems such as the Chernov–Lebowitz model, however, the symmetry is lost and no pairing rule exists.

Due to the collisions of the disks with the reflecting walls the phase volume of the Chernov–Lebowitz model shrinks continuously and the sum of all Lyapunov exponents, which equals the logarithmic phase-space volume contraction rate, is negative. Consequently, the phase-space distribution collapses onto a multifractal strange attractor with vanishing phase volume. The fractal dimension of this strange attractor can be estimated with the conjecture of Kaplan and Yorke,[11]

$$D_{KY} = n + \frac{\sum_{l=1}^{n} \lambda_l}{|\lambda_{n+1}|} \tag{1.7}$$

where n is the largest integer for which $\sum_{l=1}^{n} \lambda_l \geqslant 0$. D_{KY} is the dimension of a phase-space object, which neither shrinks nor grows and for which the natural measure is conserved by the flow. It provides a good estimate of the information dimension D_1 of the multifractal attractor.

In Section 2 we outline our method for the computation of the Lyapunov exponents for the Chernov–Lebowitz model. We present our simulation results in Section 3 and summarize our conclusions in Section 4.

2. METHOD

For the computation of full Lyapunov spectra for smooth dynamical systems the algorithm of Benettin *et al.*[12] has become a standard. It follows the time evolution of a reference trajectory and of a complete set of tangent vectors by solving the original and the linearized equations of motion, respectively. Periodical reorthonormalization of the tangent vectors avoids the collapse of all tangent vectors into the direction of fastest growth. By averaging the logarithmic expansion and contraction rates of the tangent vectors one obtains the Lyapunov exponents. However, for systems with impulsive hard collisions Benettin's method must be generalized[13] to include the effect of collisions on the trajectory *and* on the tangent space vectors. In this section we consider the collision rules, which allow us to compute the complete time evolution of the tangent-space vectors.

In the Chernov–Lebowitz model the free streaming is interrupted by impulsive collisions of the particles either with other particles or with the walls. The free streaming and the particle-particle collisions in the bulk were treated in Section III-D of ref. 13, where the same notation was used as we apply in the present work. We refer to Eqs. (39)–(42) and Eqs. (68)–(73) of ref. 13 for explicit expressions of the particle-particle collision rules in phase space and tangent space, respectively. We are left with the particle-wall collisions which will be treated next.

If particle k collides with the walls its position remains unchanged and its momentum is changed according to the reflection rule (1.3) or (1.4). The collision map $\mathbf{\Gamma}^f = \mathbf{M}(\mathbf{\Gamma}^i)$ in phase space becomes

$$\mathbf{q}_j^f = \mathbf{q}_j^i \qquad \text{for} \quad j = 1,\ldots, N \tag{2.8}$$

$$\mathbf{p}_j^f = \mathbf{p}_j^i \qquad \text{for} \quad j \neq k \tag{2.9}$$

$$\mathbf{p}_k^f = |\mathbf{p}_k^i| \begin{pmatrix} \cos\theta^f \\ \sin\theta^f \end{pmatrix} = |\mathbf{p}_k^i| \begin{pmatrix} \cos[f_a(\theta^i)] \\ \sin[f_a(\theta^i)] \end{pmatrix} \tag{2.10}$$

where $a = t$ or b refers to they top or the bottom wall, respectively. Throughout, the superscripts i and f refer to states immediately before and after a collision, respectively.

Next, we derive the corresponding transformation rules for the tangent space vectors $\delta\mathbf{\Gamma}$ at particle-wall collisions. Let us assume that a collision

takes place at the phase point Γ at time τ_c. Then a satellite trajectory, displaced by the infinitesimal vectors $\delta\Gamma$, collides at a different phase point $\Gamma+\delta\Gamma_c$ and at a different time $\tau_c+\delta\tau_c$. A linear approximation in phase space *and* in time yields[13]

$$\delta\Gamma^f=\frac{\delta\mathbf{M}}{\delta\Gamma}\cdot\delta\Gamma^i+\left[\frac{\partial\mathbf{M}}{\partial\Gamma}\cdot\mathbf{F}(\Gamma^i)-\mathbf{F}(\mathbf{M}(\Gamma^i))\right]\delta\tau_c \tag{2.11}$$

where $\mathbf{F}$ is the right hand side of the equation of motion during the free streaming,[13] and $\partial\mathbf{M}/\partial\Gamma$ is the matrix of the derivatives of the collision map with respect to the phase-space coordinates. Obviously, the delay time $\delta\tau_c$ is a function of the phase point Γ^i and of the tangent vector $\delta\Gamma^i$. For a disk-wall collision of the kth particle the time delay $\delta\tau_c$ is given by

$$\delta\tau_c=-\frac{(\delta\mathbf{q}_k\cdot\mathbf{n})}{(\mathbf{p}_k/m\cdot\mathbf{n})} \tag{2.12}$$

Here, $\mathbf{n}$ is a unit vector perpendicular to the hard wall and pointing into the simulation box. Since the reflection rules (2.8)–(2.10) for the momentum components are independent of the position of the particle, the matrix $\partial\mathbf{M}/\partial\Gamma$ has the form

$$\frac{\partial\mathbf{M}}{\partial\Gamma}=\begin{pmatrix}\mathbf{1} & \mathbf{0}\\ \mathbf{0} & \mathbf{B}\end{pmatrix} \tag{2.13}$$

where $\mathbf{1}$ is the $2N\times 2N$ unit matrix, and $\mathbf{0}$ is the $2N\times 2N$ zero matrix. $\mathbf{B}$ is the matrix of the derivatives of the outgoing momenta with respect to the incoming momenta. Only the components of $\mathbf{B}$ corresponding to the colliding particle k are different from zero. From (2.11) the following transformation rules for the tangent vectors can be deduced:

$$\delta\mathbf{q}_j^f=\delta\mathbf{q}_j^i \qquad \text{for} \quad j\neq k \tag{2.14}$$

$$\delta\mathbf{p}_j^f=\delta\mathbf{p}_j^i \qquad \text{for} \quad j\neq k \tag{2.15}$$

$$\delta\mathbf{q}_k^f=\delta\mathbf{q}_k^i-(\mathbf{p}_k^f-\mathbf{p}_k^i)\,\delta\tau_c \tag{2.16}$$

$$\delta\mathbf{p}_k^f=\tilde{\mathbf{B}}\cdot\delta\mathbf{p}_k^i \tag{2.17}$$

where $\tilde{\mathbf{B}}$ is the 2×2 matrix

$$\tilde{B}_{\alpha\beta}=\frac{\partial p_\alpha^f}{\partial p_\beta^i} \qquad \alpha,\beta\in\{x,y\} \tag{2.18}$$

For notational convenience we have omitted here the index k indicating the colliding particle. From the reflection rule $\theta^f = f(\theta^i)$ we obtain

$$\tilde{B}_{xx} = \frac{1}{p^2}\left(p^i_x p^f_x + p^i_y p^f_y \frac{\partial f}{\partial \theta^i}\right), \qquad \tilde{B}_{xy} = \frac{1}{p^2}\left(p^i_y p^f_x - p^i_x p^f_y \frac{\partial f}{\partial \theta^i}\right) \tag{2.19}$$

$$\tilde{B}_{yx} = \frac{1}{p^2}\left(p^i_x p^f_y + p^i_y p^f_x \frac{\partial f}{\partial \theta^i}\right), \qquad \tilde{B}_{yy} = \frac{1}{p^2}\left(p^i_y p^f_y - p^i_x p^f_x \frac{\partial f}{\partial \theta^i}\right) \tag{2.20}$$

where $p = |\mathbf{p}^i_k|$. Differentiating the reflection rules (1.3) and (1.4) we obtain for the c-rule:

$$\frac{\partial f}{\partial \theta^i} = -c \qquad \text{top and bottom wall} \tag{2.21}$$

and for the b-rule:

$$\frac{\partial f}{\partial \theta^i} = -\frac{\theta^i + b}{[(\pi+b)^2 - \theta^i(\theta^i + 2b)]^{1/2}} \qquad \text{top wall} \tag{2.22}$$

$$\frac{\partial f}{\partial \theta^i} = -\frac{\theta^i + \pi + b}{[(\pi+b)^2 - (\theta^i + \pi)(\theta^i + \pi + 2b)]^{1/2}} \qquad \text{bottom wall} \tag{2.23}$$

Combining the free streaming with the transformations for the disk-disk and the disk-wall collisions, we are now able to follow the exact time evolution of the trajectory and of the tangent-space vectors.

We note that Lyapunov spectra can also be calculated by using small but finite separations between the reference trajectory and the satellite trajectories instead of infinitesimal tangent vectors. We have used this approach to check the results of our numerical computations. However, the finite-difference method is computationally far less efficient then the infinitesimal, because for every Lyapunov exponent a full satellite trajectory must be determined, whereas in the infinitesimal approach most of the computational steps are identical for all tangent vectors and need to be performed only once.

3. RESULTS AND DISCUSSION

In this section we use the algorithm derived in the last section to calculate full Lyapunov spectra for the N-particle Chernov–Lebowitz model for various strain rates. In all our numerical computations we used units for which the particle mass m, the disk diameter σ and the Boltzmann constant k_B are equal to unity. Time is measured in units of $(m\sigma^2 N/K)^{1/2}$,

where K is the total kinetic energy of the system. Since after a scaling of the momenta the system retraces the same trajectory in configuration space albeit with a different rate, we restrict ourselves to simulations at $K = N$. The Lyapunov exponents are proportional to $\sqrt{K}$. We use the same square geometry as used in ref. 7. The density of the system is defined as $\rho = N/A$, where $A = L^2$ is the area of the simulation box. Obviously, the centers of the disks are confined to an area $L(L-\sigma)$. As usual in hard disk simulations we follow a collision-to-collision approach.[14] For computational efficiency we divide the simulation box into small cells and use neighbor lists.[15] To start we position the disk centers on the sites of a triangular lattice and choose the momenta at random from a Gaussian distribution with zero mean. Then the total momentum is set to zero and the momenta are rescaled to obtain the kinetic energy $K = N$.

We computed the maximum Lyapunov exponent of the 200-disk system at the density $\rho = 0.12733$ studied by Chernov and Lebowitz in ref. 7. The results for various model parameters are summarized in Table 1. Here, γ is the shear rate computed by fitting a straight line to the velocity profile. We used the same driving parameters c and b as Chernov and Lebowitz in their original work. Fig. 2 shows λ_1 as a function of the shear rate γ for the c- and b-models. The errors $\pm\Delta\lambda$ are indicated by the error bars and are less than 0.5%. They were estimated from the convergence of the exponents, plotted as a function of the simulation time, such that the time-dependent exponents did not deviate more than $\pm\Delta\lambda$ from their converged values λ during the second half of the simulation run. For both models the maximum Lyapunov exponent decreases with the shear rate. The similarity of these curves for both variants of the model indicates that

Table 1. Maximum Lyapunov Exponent λ_1 and Shear Rate γ of the c-Model and the b-Model for Various Parameters c and b at the Density $\rho = 0.12733$[a]

c-model			b-model		
c	γ	λ_1	b	γ	λ_1
0.90	0.0233	1.034	200.0	0.0256	1.029
0.93	0.0178	1.053	100.0	0.0142	1.061
0.95	0.0133	1.062	70.0	0.0085	1.067
0.97	0.0082	1.069	45.5	0.0051	1.074
0.98	0.0051	1.075	26.7	0.0044	1.073
0.99	0.0033	1.074	12.5	0.0025	1.075

[a] The system consists of 200 disks. The parameters are the same as in Table I of the original paper by Chernov and Lebowitz of ref. 7. The Lyapunov exponents and the shear rate are given in units of $(m\sigma^2 N/K)^{-1/2}$.

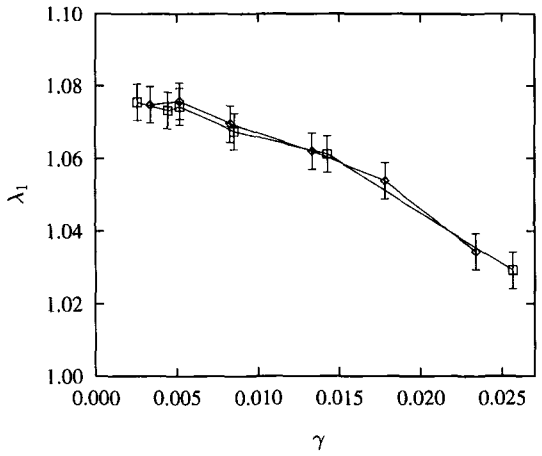

Fig. 2. Maximum Lyapunov exponent for a system of $N=200$ particles at a density of $\rho=0.12733$ corresponding to the system studied by Chernov and Lebowitz in ref. 7. The two curves refer to the c-model and the b-model, respectively. To allow a comparison of the two models the Lyapunov exponents are given as a function of the shear rate γ obtained by fitting a straight line to the velocity profile. The parameters used are listed in Table 1. The exponents and the shear rates are given in units of $(m\sigma^2 N/K)^{-1/2}$.

the different reflection rules basically lead to the same Lyapunov instability provided they generate identical shear rates.

Since the computational effort for the calculation of full Lyapunov spectra grows with the square of the particle number, we restricted ourselves to a relatively small system with $N=36$ disks for this task. Full spectra for the c-model and the b-model are shown in Figs. 3 and 4 for the density $\rho=0.6$, and in Figs. 5 and 6 for the density $\rho=0.12733$. The corresponding simulation parameters and results are summarized in Tables 2 and 3. The Lyapunov exponents are given in units of inverse time $(m\sigma^2 N/K)^{-1/2}$. Fig. 7 shows analogous spectra for a very small system containing only 4 disks at a density $\rho=0.2$. To emphasize conjugate exponent pairs, an index i is used on the abscissa for all Lyapunov spectra in these figures, such that the conjugate pair formed by the maximum and minimum exponents, $\{\lambda_1, \lambda_{4N}\}$, is associated with the index $2N$, the pair $\{\lambda_2, \lambda_{4N-1}\}$ with the index $2N-1$, and so on. Since two vanishing exponents are excluded from the ordered list of exponents prior to the definition of the pairs, there are altogether $2N-1$ pairs in each spectrum. There is no conjugate pair for the index $i=1$. Of course, the exponents are defined only for integer i. They are connected in the figures only for clarity. At least 1.4×10^6 particle-particle collisions and 1.4×10^5 particle-wall collisions occurred in each simulation. The errors of the Lyapunov exponents,

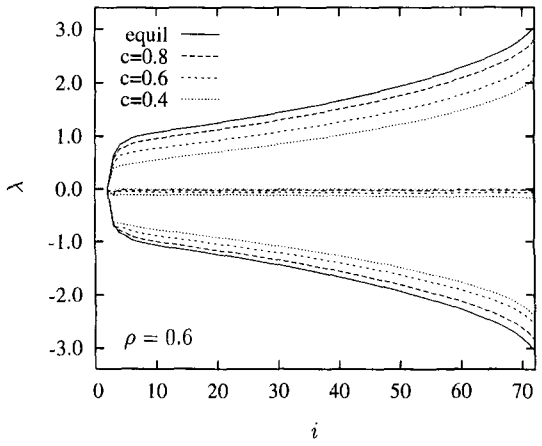

Fig. 3. Full Lyapunov spectra for the 36-particle c-model for different values of c at a density of $\rho = 0.6$. The pair sum of conjugate exponents is also indicated by the lines near the abscissa. The exponents are given in units of $(m\sigma^2 N/K)^{-1/2}$.

estimated with the method indicated above, are less than $\pm 0.2\%$ of the respective maximum exponent. Since for the driving parameters used in ref. 7 the Lyapunov exponents deviate only modestly from their equilibrium values, we used a stronger driving for our computations of the full spectra.

In the Chernov–Lebowitz model three Lyapunov exponents vanish. We verified this with high accuracy for small systems (3 to 4 particles) and

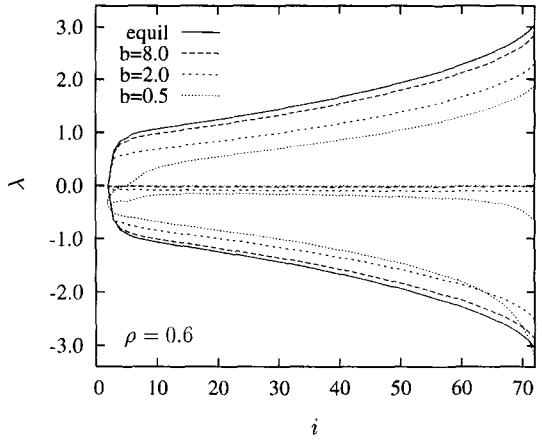

Fig. 4. Full Lyapunov spectra for the 36-particle b-model for different values of b at a density of $\rho = 0.6$. The pair sum of conjugate exponents is also indicated by the lines near the abscissa. The exponents are given in units of $(m\sigma^2 N/K)^{-1/2}$.

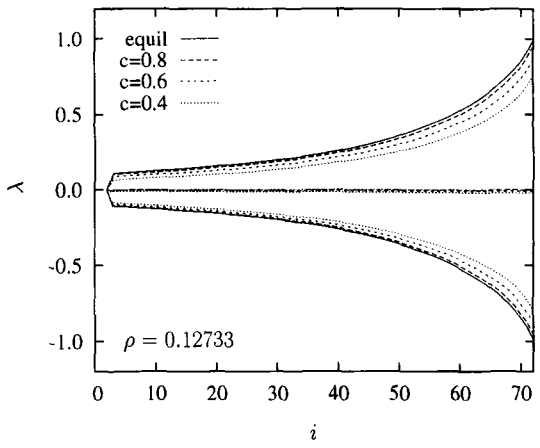

Fig. 5. Full Lyapunov spectra for the 36-particle c-model for different values of c at a density of $\rho = 0.12733$. The pair sum of conjugate exponents is also indicated by the lines near the abscissa. The exponents are given in units of $(m\sigma^2 N/K)^{-1/2}$.

various driving parameters c and b. One exponent vanishes due to the neutral expansion behavior in the direction of the flow. A second exponent vanishes due to the conservation of kinetic energy. However, there is no other conserved quantity to account for the third vanishing exponent. This exponent equals zero due to the invariance of the system to translations in the x-direction. Such a translation corresponds to the tangent vector

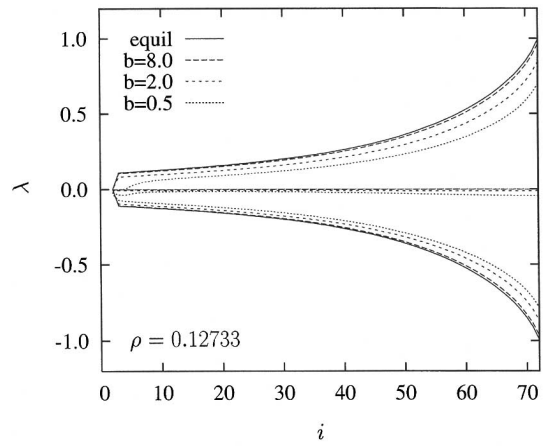

Fig. 6. Full Lyapunov spectra for the 36-particle b-model for different values of b at a density of $\rho = 0.12733$. The pair sum of conjugate exponents is also indicated by the lines near the abscissa. The exponents are given in units of $(m\sigma^2 N/K)^{-1/2}$.

Table 2. Shear Rate γ, Viscosity η, Kaplan–Yorke Dimension D_{KY}, Kolmogorov–Sinai Entropy per Particle h_K/N, and Maximum Lyapunov Exponent λ_1 of the c-Model and the b-Model at the Density $\rho = 0.12733$

c-model						b-model					
c	γ	η	D_{KY}	h_K/N	λ_1	b	γ	η	D_{KY}	h_K/N	λ_1
0.40	0.122	0.240	140.77	0.447	0.752	0.5	0.123	0.209	138.50	0.398	0.697
0.45	0.117	0.256	141.34	0.470	0.780	0.7	0.121	0.222	139.60	0.422	0.728
0.50	0.111	0.278	141.82	0.492	0.811	1.0	0.116	0.245	140.66	0.453	0.762
0.55	0.104	0.297	142.22	0.513	0.835	1.4	0.111	0.259	141.52	0.481	0.800
0.60	0.097	0.316	142.58	0.532	0.862	2.0	0.101	0.286	142.30	0.516	0.845
0.65	0.088	0.333	142.88	0.552	0.888	2.8	0.090	0.306	142.85	0.544	0.879
0.70	0.080	0.346	143.14	0.569	0.913	4.0	0.075	0.333	143.28	0.573	0.918
0.75	0.070	0.357	143.36	0.584	0.935	5.6	0.061	0.348	143.55	0.594	0.945
0.80	0.059	0.360	143.55	0.599	0.952	8.0	0.048	0.358	143.74	0.607	0.963
0.85	0.047	0.363	143.71	0.610	0.967	11.2	0.037	0.353	143.85	0.617	0.976
0.90	0.033	0.369	143.85	0.621	0.981	16.0	0.026	0.386	143.92	0.624	0.984
0.95	0.018	0.343	143.95	0.627	0.987	22.4	0.019	0.391	143.95	0.626	0.989
100	0.000	—	144.00	0.630	0.994	∞	0.000	—	144.00	0.630	0.994

Table 3. Shear Rate γ, Viscosity η, Kaplan–Yorke Dimension D_{KY}, Kolmogorov–Sinai Entropy per Particle h_K/N, and Maximum Lyapunov Exponent λ_1 of the c-Model and the b-Model at the Density $\rho = 0.6$

c-model						b-model					
c	γ	η	D_{KY}	h_K/N	λ_1	b	γ	η	D_{KY}	h_K/N	λ_1
0.40	0.330	0.876	135.67	2.029	2.077	0.5	0.349	0.729	129.77	1.655	1.875
0.45	0.321	0.929	137.03	2.149	2.159	0.7	0.343	0.771	131.89	1.771	1.938
0.50	0.309	0.997	138.21	2.274	2.249	1.0	0.333	0.839	134.24	1.938	2.042
0.55	0.295	1.063	139.25	2.395	2.342	1.4	0.321	0.910	136.40	2.115	2.148
0.60	0.280	1.122	140.16	2.514	2.429	2.0	0.299	1.023	138.51	2.329	2.299
0.65	0.262	1.185	140.96	2.632	2.518	2.8	0.274	1.123	140.19	2.531	2.446
0.70	0.240	1.256	141.65	2.754	2.611	4.0	0.240	1.230	141.55	2.735	2.595
0.75	0.216	1.318	142.25	2.873	2.700	5.6	0.205	1.319	142.47	2.907	2.728
0.80	0.186	1.392	142.78	2.993	2.800	8.0	0.165	1.396	143.12	3.052	2.842
0.85	0.151	1.441	143.23	3.100	2.883	11.2	0.130	1.443	143.49	3.148	2.917
0.90	0.109	1.497	143.59	3.197	2.959	16.0	0.096	1.489	143.73	3.217	2.976
0.95	0.058	1.561	143.87	3.270	3.016	22.4	0.072	1.494	143.85	3.251	2.997
100	0.000	—	144.00	3.297	3.404	∞	0.000	—	144.00	3.297	3.040

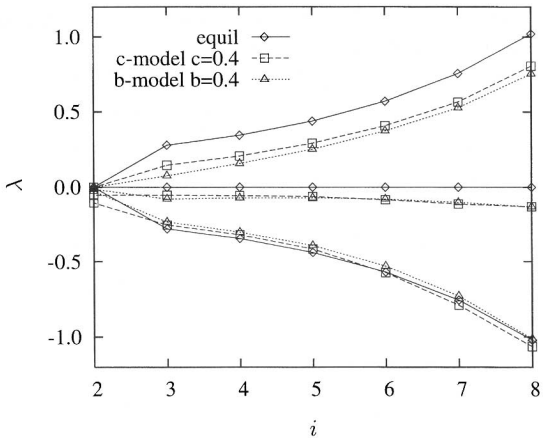

Fig. 7. Lyapunov spectra for a 4-particle system with density $\rho = 0.2$. Equilibrium and nonequilibrium states for the b- and c-model are considered. Each particle is involved in more than 10 million collisions with other particles, and more than five million collisions with the walls. The error for each exponent is less than ± 0.001, and less than ± 0.002 for each pair sum. The pair sum of conjugate exponents is also indicated by the lines near the abscissa. The exponents are given in units of $(m\sigma^2 N/K)^{-1/2}$.

$\delta\Gamma = \{\delta\mathbf{q}_1, \delta\mathbf{q}_2, \delta\mathbf{q}_3, \ldots, \delta\mathbf{q}_N, \delta\mathbf{p}_1, \delta\mathbf{p}_2, \delta\mathbf{p}_3, \ldots, \delta\mathbf{p}_N\}$, with $\delta\mathbf{q}_j = \{1, 0\}$ and $\delta\mathbf{p}_j = \{0, 0\}$. This tangent vector does not change with time as can be seen by direct insertion into the equations of motion and into the transformation rules for disk-disk and disk-wall collisions. Consequently, the Lyapunov exponent corresponding to this tangent vector vanishes. The existence of this third vanishing exponent is particularly obvious for the four-particle spectra shown in Fig. 7. There, this exponent is located at $i = 2$ and is paired with another exponent, which is negative for nonequilibrium steady states, and zero in equilibrium.

In all figures the full line denotes the equilibrium spectrum of the Lyapunov exponents which is completely symmetrical with vanishing pair sums. This symmetry is destroyed as the driving is turned on and the pair sums are shifted towards more negative values. Then the sum of the Lyapunov exponents is negative and exactly equal to the phase-space contraction rate. The latter has been calculated in ref. 7 by averaging the logarithm of the compression factor m for particle-wall collisions. If a particle is reflected at the rigid boundaries the phase space is compressed by the factor[7]

$$m = \left| \frac{\sin\theta^f}{\sin\theta^i} \frac{df}{d\theta^i} \right| \tag{3.24}$$

The shift of the Lyapunov spectra is accompanied by a reduction of the dimension of the occupied phase space.

An inspection of the nonequilibrium spectra in Figs. 3 to 7 reveals that the conjugate pairing rule is not obeyed. In these figures the pair sums for conjugate exponent pairs are indicated by the same symbols as the original spectra. They are clearly *not* on a horizontal line and vary considerably with i. This is clearly seen also for the smallest system of our study, the four-particle case of Fig. 7. The deviations, particularly for large indexes, significantly exceed the numerical uncertainty for the pair sum, which is ± 0.002.

The deviations from the pairing rule are particularly pronounced for strong driving. This result does not come as a surprise, since the systems are inhomogenously driven in the sense that particles interacting with the boundaries and bulk particles are treated differently. This pairing asymmetry has already been observed in another inhomogeneous model for planar shear flow between two moving thermostatted walls.[16] There the asymmetry is even much more pronounced and affects mainly the few most negative exponents associated with the thermostatted degrees of freedom. The way vanishing exponents influence the pairing rule has been clarified for homogeneous systems in refs. 13 and 10. Analogous considerations apply also to the inhomogeneous b- and c-models considered here.

Due to the higher collision rate at high densities the Lyapunov exponents are larger for $\rho = 0.6$ than for $\rho = 0.12733$. Moreover, at low densities the spectra have a stronger curvature. At larger densities a step between the last vanishing exponent and the first strictly positive exponent can be observed. However, this step does not persist in the thermodynamical limit.[13] As shown in Figs. 3 and 4 the step is retained for moderate driving parameters but is smoothed out for very strong driving. This was observed also in the case of thermostatted hard disks subjected to a color field.[13]

For moderate parameters c and b the positive exponents are shifted more than the negative exponents by the driving boundaries Simultaneously, the positive as well as the negative exponents decrease in magnitude. Of course, to make the sum of all exponents negative, the shift of the positive exponents must be larger. This effect was observed also in the color conductivity model and in the externally driven Lorentz gas at high and intermediate densities.[17] Thus, the driving makes the system less chaotic. This is reflected also in a decreasing Kolmogorov–Sinai entropy h_K per particle, calculated from the sum of all positive Lyapunov exponents and shown in Figs. 8 and 9 for the densities $\rho = 0.127$ and $\rho = 0.6$, respectively. Qualitatively this can be understood by noting that during the wall collisions the particle momenta are reoriented closer to the x-direction.

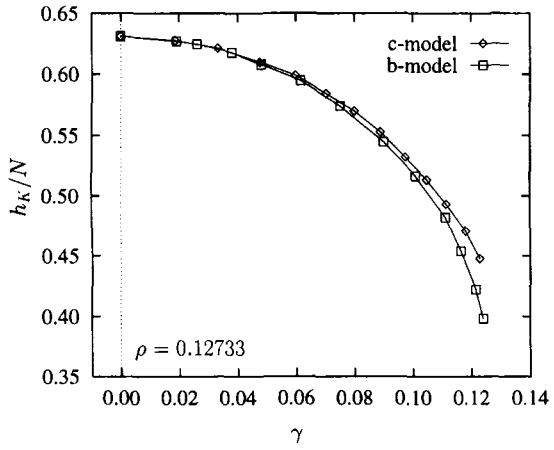

Fig. 8. Kolmogorov–Sinai entropy per particle for the 36-particle system as a function of the shear rate γ at a density of $\rho = 0.12733$. h_K is given in units of $(m\sigma^2 N/K)^{-1/2}$.

This increases the order and reduces the chaoticity. As can be inferred from the data shown in the figures the Kolmogorov–Sinai entropy does not depend on the specific reflection rule used to generate the shear flow. Furthermore, it is interesting to note that for the *b*-model the number of negative exponents may increase for strong driving, as may be inferred from Figs. 4 and 6. No analogous behaviour is observed for the *c*-model under similar nonequilibrium conditions.

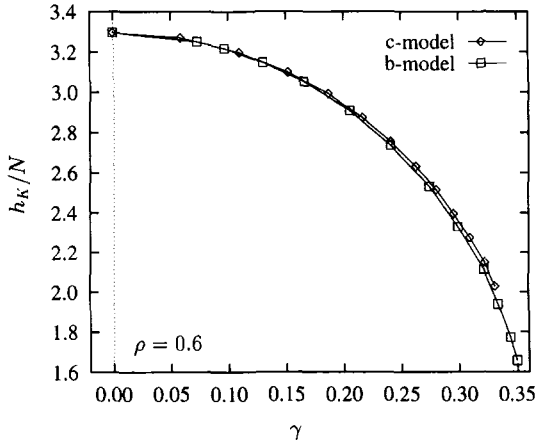

Fig. 9. Kolmogorov-Sinai entropy per particle for the 36-particle system as a function of the shear rate γ at a density of $\rho = 0.6$. h_K is given in units of $(m\sigma^2 N/K)^{-1/2}$.

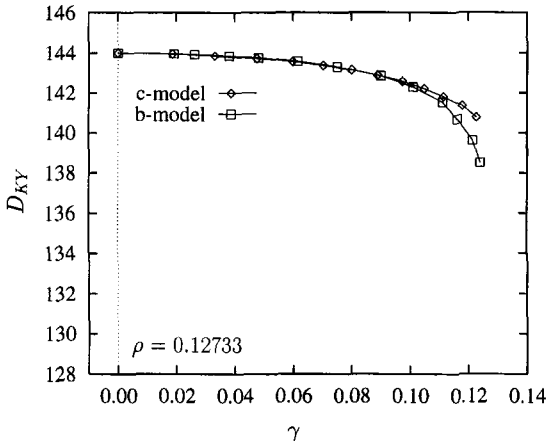

Fig. 10. Kaplan–Yorke dimension of the 36-particle system as a function of the shear rate γ at a density of $\rho = 0.12733$.

Figures 10 and 11 show the Kaplan–Yorke dimension as a function of the shear rate for the 36-particle system at $\rho = 0.127$ and $\rho = 0.6$. As observed already for h_K and λ_1, also the Kaplan–Yorke dimension D_{KY} does not depend on the specific reflection rule. For small-enough shear rates $\gamma < 0.06$ the dimensionality loss $\Delta D = 4N - D_{KY}$ is proportional to γ^2 as suggested by a expansion of ΔD in powers of γ. It is surprising that this quadratic behavior persists only over such a small range of γ, much smaller

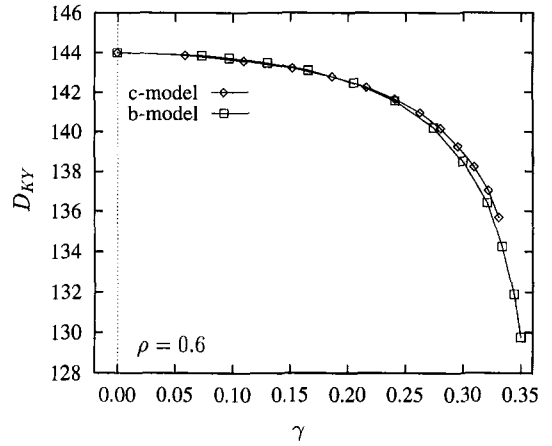

Fig. 11. Kaplan–Yorke dimension of the 36-particle system as a function of the shear rate γ at a density of $\rho = 0.6$.

than for thermostatted homogeneous[18] or inhomogeneous[16] driving. Moreover, for a given shear rate γ the dimensionality loss ΔD is larger for low than for high densities.

4. CONCLUSION

In this paper we evaluated Lyapunov spectra for the Chernov–Lebowitz model for boundary driven shear flow. Although the system is strictly energy conserving it is dissipative and is subjected to a phase-space contraction. The phase space distribution of such a system collapses onto a fractal object with zero volume and a dimension less than the phase-space dimension. The information dimension of the system has been estimated with the conjecture of Kaplan and Yorke. We found that the dimensionality loss ΔD increases with the shear rate γ. In equilibrium the Lyapunov spectra of the model are similar to the spectra of hard disks. In nonequilibrium states rather strong driving is necessary to shift the spectra significantly towards more negative values. Since the driving is inhomogeneous, the Lyapunov spectra do not obey the conjugate pairing symmetry. The chaotic properties of the model are rather independent from the specific reflection rule (b- or c-model) provided it induces the same linear velocity profile.

ACKNOWLEDGMENTS

The authors gratefully acknowledge the financial support from the *Fonds zur Förderung der wissenschaftlichen Forschung* under grants P09677 and P11428, and the generous allocation of computer resources by the Computer Center of the University of Vienna.

REFERENCES

1. D. J. Evans and G. P. Morriss, *Statistical Mechanics of Nonequilibrium Liquids*, Academic Press, London (1990).
2. W. G. Hoover, *Computational Statistical Mechanics*, Elsevier, Amsterdam (1991).
3. H. A. Posch and W. G. Hoover, *Phys. Rev. A* **39**:2175 (1989).
4. W. G. Hoover, D. J. Evans, R. B. Hickman, A. J. C. Ladd, W. T. Ashurst, and B. Moran, *Phys. Rev. A* **22**:1690 (1980).
5. D. J. Evans and G. P. Morriss, *Phys. Rev. A* **30**:1528 (1984).
6. H. A. Posch, W. G. Hoover, and B. L. Holian, *Ber. Bunsenges. Phys. Chem.* **94**:250 (1990).
7. N. I. Chernov and J. L. Lebowitz, *Phys. Rev. Lett.* **75**:2831 (1995); and *J. Stat. Phys.* **86**:(1997).
8. V. I. Oseledec, *Trans. Moscow Math. Soc.* **19**:197 (1968).
9. D. J. Evans, E. G. D. Cohen, and G. P. Morriss, *Phys. Rev. A* **42**:5990 (1990).

10. C. P. Dettmann and G. P. Morriss, *Phys. Rev. E* **53**:R5545 (1996).
11. J. Kaplan and J. A. Yorke, in *Functional Differential Equations and Approximation of Fixed Points*, edited by H. O. Peitgen and H. O. Walther, Springer Verlag, Heidelberg (1979).
12. G. Benettin, L. Galgani, A. Giorgilli, and J.-M. Strelcyn, *Meccanica* **15**:9 (1980).
13. Ch. Dellago, H. A. Posch, and W. G. Hoover, *Phys. Rev. E.* **53**:1485 (1996).
14. F. J. Vesely, *Computational Physics, An Introduction*, Plenum Press, New York (1994).
15. M. P. Allen and D. J. Tildesley, *Computer Simulation of Liquids*, Oxford University Press, Oxford (1987).
16. H. A. Posch and W. G. Hoover, in *Molecular Liquids: New perspectives in Physics and Chemistry*, edited by J. J. Teixeira-Dias, NATO ASI 378B, 527, Kluwer Academic Publishers (1992).
17. Ch. Dellago, L. Glatz, and H. A. Posch, *Phys. Rev. E.* **52**:4817 (1995).
18. W. G. Hoover and H. A. Posch, *Phys. Rev. E.* **49**:1913 (1994).